Available online at www.sciencedirect.com

ScienceDirect

IFAC PapersOnline CONFERENCE PAPER ARCHIVE

IFAC PapersOnLine 51-29 (2018) 274–280

Semiglobal Exponential Stability of a Counter-Current and Co-Current Guidance Scheme

Walter Caharija [*,**] **Esten I. Grøtli** [***] **Kristin Y. Pettersen** [*]

[*] *NTNU AMOS, Dept. of Eng. Cybernetics, Trondheim, Norway, e-mail: {Walter.Caharija, Kristin.Y.Pettersen}@itk.ntnu.no*

[**] *SINTEF Ocean, Trondheim, Norway, e-mail: Walter.Caharija@sintef.no*

[***] *SINTEF Digital, Trondheim, Norway, e-mail: EstenIngar.Grotli@sintef.no*

Abstract: A control technique for counter-current and co-current guidance of underactuated marine vehicles is revisited and stronger stability properties are shown. In particular, the stronger property of uniform semiglobal exponential stability is shown for the complete multiple-equilibria closed loop system, that has previously been shown to be uniformly semiglobally asymptotically stable and uniformly locally exponentially stable. Compared to the original proof, the analysis presented in this paper does not invoke the theory developed for cascaded systems; it follows instead a direct approach where a Lyapunov function for the full system is identified. This shows that analysing stability of a complex non-linear system by means of proper Lyapunov function candidates can yield significant results, leaving however the designer with the challenging task of identifying the right candidate. The theory is supported by simulations.

Keywords: underactuated vessel, ocean currents, semiglobal stability, multiple equilibria

1. INTRODUCTION

The maritime industry regards automation and robotics as key technologies to increase reliability, effectiveness, safety and sustainability of operations related to fish farming, fishing, offshore wind power production, offshore oil & gas and environmental monitoring. Such activities are significantly affected by wind, waves and sea currents that can seriously affect the manoeuvrability of ships and vehicles, and pose a threat to the safety of the crews involved. Reducing sea loads has therefore been one of the priorities for the marine control field of research and important solutions have been developed such as dynamic positioning with weather-vaning. Furthermore, present and future challenges are continuously pushing the field to improve existing solutions, and bring up new ideas.

Weather optimal station-keeping has been subject of extensive research: Fossen and Strand (2001) and later Kjerstad and Breivik (2010) proposed to move the vessel along a circle arc with constant radius and letting the bow of the ship point towards the origin of the circle. The bow of the ship is automatically turned against the mean environmental disturbance, analogously to a pendulum subject to gravity. More recently, Kim et al. (2016) presented a weather optimal station-keeping controller, that does not rely on measuring or estimating the environmental forces. The controller is derived based on vectorial backstepping and it provides a virtual rotation center for weathervaning of the vessel. A similar approach was taken in Kim et al. (2017) for weathervaning control of two surface vessels in tandem, but with the need of an additional coordination control scheme between the vessels to suppress relative motion and improve safety.

Sea currents have challenged seafarers since the early days of coastal navigation since proper handling and estimation of the currents may determine the safe and successful accomplishment of an operation at sea. Hence several solutions such as observers, robust adaptive techniques and prediction algorithms have been developed, often as part of more complex control systems (Encarnação et al., 2000; Do et al., 2004; Antonelli, 2007; Smith et al., 2011; Jouffroy et al., 2011; Batista et al., 2012; Indiveri et al., 2012). Currents strongly affect also the popular line-of-sight (LOS) guidance law to which the research community responded by adding robustness via velocity measurements (Aguiar and Pascoal, 1997) and integral action (integral line-of-sight, ILOS) (Børhaug et al., 2008; Breivik and Fossen, 2009; Caharija et al., 2016). Furthermore, Fossen and Lekkas (2017) presented two robust ILOS path-following controllers, while Zheng et al. (2017) proposed and adaptive LOS guidance law coupled with a current observer to make the vehicle produce a variable sideslip angle to compensate for the drift force for any parametric curved-path. Current disturbances are also taken into account and estimated in Paliotta et al. (2016) where a trajectory tracking control strategy based on input-output feedback linearisation was developed.

This work deals with steering a marine vessel against the ocean current or with the ocean current. A guidance law capable of steering the vehicle with the current can help benefiting from the drift when system efficiency and

Supported by the Research Council of Norway through the Centres of Excellence funding scheme (project number 223254) and the Strategic University Program (project number 192427).

10.1016/j.ifacol.2018.09.515

endurance are relevant, such as in Smith et al. (2011). Vice-versa, a control system that steers the vessel against the current can be integrated into weather optimal heading/positioning control systems where station keeping is fundamental or when the goal is to lose as little ground as possible and minimize the overall load, when affected by strong overwhelming disturbances.

This paper revisits the control techniques for counter-current and co-current guidance of underactuated marine vehicles from Caharija et al. (2013, 2014) and shows stronger stability properties. In particular, the analysis shows uniform semiglobal exponential stability (USES) for the complete multiple-equilibria closed loop system, while Caharija et al. (2014) concluded uniform semiglobal asymptotical stability (USAS) and uniform local exponential stabilty (ULES), which are weaker stability properties. Compared to the original proof, the analysis presented in this paper does not invoke the theory developed for cascaded systems from Chaillet and Loría (2008) that was heavily exploited in Caharija et al. (2014); it follows instead a direct approach where a Lyapunov function for the full system is identified. The results show that identifying the right Lyapunov function candidate when testing the stability of a non-linear system with multiple equilibriums, although a very demanding task, can be very advantageous. The theoretical results are supported by simulations where a different model compared to Caharija et al. (2013, 2014) is used: in this case the model is a very realistic representation of the commercially available HUGIN AUV while in Caharija et al. (2013, 2014) the supply vessel model from Fredriksen and Pettersen (2004) was used.

The paper is organized as follows: Section 2 presents the control plant model of the vehicle, Section 3 identifies the control objective and Section 4 presents the strategy that solves the control task. The main result is stated in Section 5 and proven in Section 6. Simulation results and conclusions are given in Section 7 and Section 8, respectively.

2. THE VEHICLE MODEL

The class of port/starboard symmetric marine vehicles described by the 3-DOF maneuvering model presented in Fossen (2011) is considered:

$$\dot{\boldsymbol{p}} = \boldsymbol{R}(\psi)\boldsymbol{\nu}_r + \boldsymbol{V}_c, \tag{1}$$

$$\boldsymbol{M}\dot{\boldsymbol{\nu}}_r + \boldsymbol{C}(\boldsymbol{\nu}_r)\boldsymbol{\nu}_r + \boldsymbol{D}\boldsymbol{\nu}_r = \boldsymbol{B}\boldsymbol{f}. \tag{2}$$

The state of the surface vessel is given by $[\boldsymbol{p}^T, \boldsymbol{\nu}_r^T]^T$ where $\boldsymbol{p} \triangleq [x, y, \psi]^T$ is the position and the orientation of the vehicle with respect to the inertial frame i. As shown in Caharija et al. (2016), in navigation problems involving irrotational ocean currents it is useful to describe the state of the vessel with the relative velocity vector: $\boldsymbol{\nu}_r = [u_r, v_r, r]^T$. The vector $\boldsymbol{\nu}_r$ is defined in the body frame b, where u_r is the relative surge velocity, v_r is the relative sway velocity and r is the yaw rate. The model (1-2) describes the kinematics and dynamics of surface vessels as well as underwater vehicles moving in the horizontal plane, and describes the effect of environmental disturbances as an irrotational ocean current $\boldsymbol{V}_c$ defined in the inertial frame. It satisfies the following assumption:

Assumption 1. The ocean current $\boldsymbol{V}_c$ is constant, unknown, irrotational and bounded. Hence, $\boldsymbol{V}_c \triangleq [V_x, V_y, 0]^T$ and there exists a constant $V_{\max} > 0$ such that $V_{\max} \geq \sqrt{V_x^2 + V_y^2}$.

Since $\dot{\boldsymbol{V}}_c = \boldsymbol{0}$ by this assumption and since $\boldsymbol{\nu}_c = \boldsymbol{R}(\psi)\boldsymbol{V}_c = [u_c, v_c, 0]^T$ in b, then $\dot{\boldsymbol{\nu}}_c$ becomes:

$$\dot{\boldsymbol{\nu}}_c = [rv_c, -ru_c, 0]^T. \tag{3}$$

The vector $\boldsymbol{f} \triangleq [T_u, T_r]^T$ is the control input vector, containing the surge thrust T_u and the rudder angle T_r. Notice that the model (1-2) is underactuated in its configuration space since it has fewer control inputs than DOFs. The matrix $\boldsymbol{M} = \boldsymbol{M}^T > 0$ is the mass and inertia matrix and includes hydrodynamic added mass. The matrix $\boldsymbol{C}(\boldsymbol{\nu}_r)$ is the Coriolis and centripetal matrix, $\boldsymbol{D} > 0$ is the hydrodynamic damping matrix and $\boldsymbol{B} \in \mathbb{R}^{3\times 2}$ is the actuator configuration matrix. The structure of the matrices $\boldsymbol{R}(\psi)$, $\boldsymbol{M}$, $\boldsymbol{C}(\boldsymbol{\nu}_r)$ and $\boldsymbol{B}$ is given in Appendix A.

Assumption 2. The body-fixed coordinate frame b is considered located at a point $(x_g^*, 0)$ from the vehicle's center of gravity (CG) along the center-line of the vessel, where x_g^* is such that $\boldsymbol{M}^{-1}\boldsymbol{B}\boldsymbol{f} = [\tau_u, 0, \tau_r]^T$.

The point $(x_g^*, 0)$ exists for all port-starboard symmetric vehicles (Caharija et al., 2016). The following assumption defines the properties of the damping matrix $\boldsymbol{D}$:

Assumption 3. Damping is considered linear.

Remark 1. Nonlinear damping is not considered in order to reduce the complexity of the controllers. However, the passive nature of the non-linear hydrodynamic damping forces should enhance the directional stability of the vessel.

The hydrodynamic damping matrix $\boldsymbol{D}$ is therefore considered to have the following structure Fossen (2011):

$$\boldsymbol{D} \triangleq \begin{bmatrix} d_{11} & 0 & 0 \\ 0 & d_{22} & d_{23} \\ 0 & d_{32} & d_{33} \end{bmatrix}. \tag{4}$$

The particular structure of $\boldsymbol{D}$ is justified by symmetry arguments (Caharija et al., 2016) and Assumption 3.

2.1 The Model in Component Form

To solve nonlinear underactuated control design problems it is useful to expand (1-2) into:

$$\dot{x} = u_r \cos(\psi) - v_r \sin(\psi) + V_x, \tag{5a}$$

$$\dot{y} = u_r \sin(\psi) + v_r \cos(\psi) + V_y, \tag{5b}$$

$$\dot{\psi} = r, \tag{5c}$$

$$\dot{u}_r = F_{u_r}(v_r, r) - (d_{11}/m_{11})u_r + \tau_u, \tag{5d}$$

$$\dot{v}_r = X(u_r)r + Y(u_r)v_r, \tag{5e}$$

$$\dot{r} = F_r(u_r, v_r, r) + \tau_r. \tag{5f}$$

The expressions for $F_r(u_r, v_r, r)$, $F_{u_r}(v_r, r)$, $X(u_r)$ and $Y(u_r)$ are given in Appendix A. Notice that the functions $Y(u_r)$ and $X(u_r)$ are bounded for bounded arguments and thus the following notation is used:

$$X^{\max} \triangleq \max_{\Omega} |X(u_r)|, \tag{6}$$

where $\Omega \triangleq \{-V_{\max} \leq u_r \leq U_{rd} | U_{rd} > 0\}$ and the following assumption is introduced:

Assumption 4. The function $Y(u_r)$ satisfies:

$$Y(u_r) \leq -Y^{\min} < 0, \quad \forall u_r \in \Omega.$$

Remark 2. Assumption 4 is justified by a contradiction: $Y(u_r) \geq 0$ would imply a nominally unstable vehicle in sway which is not the case for commercial vessels by design. Furthermore, notice that no bounds are implied on u_r. The constant $U_{rd} > 0$ is a design parameter and is defined in Section 3.

3. THE CONTROL OBJECTIVE

This section formalizes the control problem solved in this paper: the control system should make the vehicle turn against the current, or follow the current, in the complementary case. In addition, the vehicle should also maintain a desired constant surge relative velocity $U_{rd} > 0$. The ocean current is considered constant and unknown as by Assumption 1. As shown in Caharija et al. (2013, 2014), to achieve counter-current guidance as well as co-current guidance, the vessel is required to align its relative velocity vector $\boldsymbol{\nu}_r$ with the current velocity vector $\boldsymbol{\nu}_c$, as shown in Figure 1. At steady state, when the two vectors are parallel, the current vector $\boldsymbol{\nu}_c$ has its sway component $v_{c,ss} = 0$. It is trivial to show that $v_{c,ss} = 0$ if and only if the vessel is pointing against the current or going with the current, i.e. if and only if $\psi_c = \text{atan2}(V_y, V_x) + k\pi,\ k \in \mathbb{Z}$. Hence, the objectives the control system should pursue can be formalized as follows:

$$\lim_{t\to\infty} v_c(t) = 0, \tag{7}$$

$$\lim_{t\to\infty} \psi(t) = \text{atan2}(V_y, V_x) + k\pi, \quad k \in \{0, 1\}, \tag{8}$$

$$\lim_{t\to\infty} u_r(t) = U_{rd}, \tag{9}$$

where $k = 0$ identifies the co-current guidance and $k = 1$ identifies the counter-current guidance. Finally, the following assumption allows the vessel to move against sea currents acting in any directions of the plane:

Assumption 5. The propulsion system is rated with power and thrust capacity such that U_{rd} satisfies $U_{rd} > V_{\max}$.

Remark 3. Notice that Assumption 5 is strictly necessary for the vessel to be able to move against the current.

Remark 4. It is trivial to show that the absolute sway velocity $v \to 0$ when the control objectives (7-8) are achieved since $v = v_r + v_c$. This property is exploited in Caharija et al. (2013) to search for the current direction. In this paper, as in Caharija et al. (2014), the signal v_c represent the error signal instead.

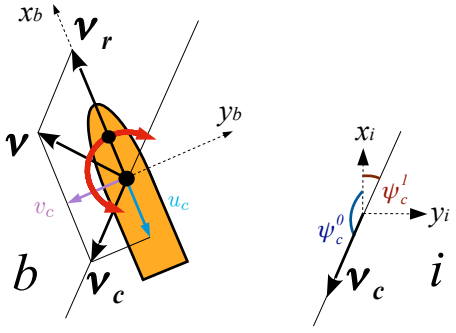

Fig. 1. The vehicle has to align its relative velocity vector $\boldsymbol{\nu}_r$ with the current vector $\boldsymbol{\nu}_c$ to perform counter-current or co-current guidance: this means holding the heading ψ_c^1 or the heading ψ_c^0, respectively.

4. THE CONTROL SYSTEM

A control system that solves the control problem defined in Section 3 is presented. First the guidance system is introduced, and then the surge and yaw controllers are added.

4.1 The Guidance Strategy

The following heading reference, first proposed in Caharija et al. (2014), is used to achieve counter-current guidance, or alternatively co-current guidance:

$$\psi_G \triangleq -\sigma v_{\text{int}}, \quad \sigma \neq 0, \tag{10a}$$

$$\dot{v}_{\text{int}} = v_c, \tag{10b}$$

where $\sigma > 0$ makes the vehicle turn against the flow and $\sigma < 0$ makes the vehicle follow the flow. The integral effect (10b) forces the vessel to search for the two directions having zero current component in the sway direction v_c at steady state, while the sign of the gain σ defines whether the counter-current course or the co-current course is the stable equilibrium point of the closed loop system. This paper shows that the simple and intuitive guidance system (10) has even stronger stability properties than first determined in Caharija et al. (2014).

Remark 5. The error signal in (10b) is the current component acting in the sway direction and it can be measured or estimated using DVL devices.

4.2 Surge and Yaw Controllers

According to (9), $u_r(t)$ should follow the desired value $u_{rd}(t) \triangleq U_{rd} > 0$. To this end the following controller is used:

$$\tau_u = -F_{u_r}(v_r, r) + \frac{d_{11}}{m_{11}} u_{rd} + \dot{u}_{rd} - k_{u_r}(u_r - u_{rd}). \tag{11}$$

The gain $k_{u_r} > 0$ is constant. The controller (11) is a feedback linearising P-controller that guarantees exponential tracking of $u_{rd}(t)$ (cf. Eq. (13) below) and is the same speed controller proposed in Caharija et al. (2014). The following controller is used to track the desired yaw angle $\psi_d \triangleq \psi_G$:

$$\tau_r = -F_r(u_r, v_r, r) + \ddot{\psi}_d - k_\psi(\psi - \psi_d) - k_r(\dot{\psi} - \dot{\psi}_d), \tag{12}$$

where $k_\psi, k_r > 0$ are constant gains. The controller (12) is a feedback linearising PD controller and makes sure that ψ and r exponentially track ψ_d and $\dot{\psi}_d$ (cf. Eq (14) below) and is the same heading controller proposed in Caharija et al. (2014).

Remark 6. Notice that $\dot{\psi}_d$ and $\ddot{\psi}_d$ are well defined if $\psi_d \triangleq \psi_G$ due to Assumption 1 and correspondingly (3).

5. MAIN RESULT

This section presents the conditions under which the proposed control system achieves the objectives (7-9). The counter-current guidance case ($\sigma > 0$) is considered only. The same derivations and conclusions can be drawn for the co-current case ($\sigma < 0$).

Theorem 1. Given an underactuated marine vehicle described by the dynamical system (5). If Assumptions 1-5 hold, the controllers (11-12), with $k_{u_r}, k_\psi, k_r > 0$,

$u_{rd} \triangleq U_{rd}$ and $\psi_d \triangleq \psi_G$, guarantee achievement of the control objectives (7-9) with USES properties. The USES properties hold on the parameter set $\Theta \triangleq \{\sigma > 0\}$.

Proof. The proof of Theorem 1 is given in Section 6. □

6. PROOF OF THEOREM 1

The proof follows along the lines of Caharija et al. (2014), without however invoking the theory developed for cascaded systems in Chaillet and Loría (2008). Instead, in this paper, the proof follows a direct approach and identifies a Lyapunov function for the full system, showing stronger stability properties. The actuated surge and yaw dynamics of the vehicle are considered first. The closed loop surge subsystem is obtained combining (5d) with (11) and given $\tilde{u}_r \triangleq u_r - U_{rd}$, the $\tilde{u}_r$ dynamics become:

$$\dot{\tilde{u}}_r = -\left(\frac{d_{11}}{m_{11}} + k_{u_r}\right)\tilde{u}_r, \tag{13}$$

where $d_{11}, m_{11}, k_{u_r} > 0$. The $\tilde{u}_r$ subsystem is clearly uniformly globally exponentially stable (UGES). Therefore, the control goal (9) is achieved exponentially in any ball of initial conditions.

The yaw ψ, r subsystem is obtained from (5c) and (5f) in closed loop configuration with (12). Given the error variables $\tilde{\psi} \triangleq \psi - \psi_d$ and $\tilde{r} \triangleq r - \dot{\psi}_d$, the dynamics of $\tilde{\psi}$ and $\tilde{r}$ are:

$$\dot{\boldsymbol{\xi}} = \begin{bmatrix} 0 & 1 \\ -k_\psi & -k_r \end{bmatrix} \boldsymbol{\xi} \triangleq \boldsymbol{\Sigma}\boldsymbol{\xi}, \tag{14}$$

where $\boldsymbol{\xi} \triangleq [\tilde{\psi}, \tilde{r}]^T$. The system (14) is linear and time-invariant. Furthermore, since the gains k_ψ, k_r are strictly positive, the system matrix $\boldsymbol{\Sigma}$ is Hurwitz and hence the origin $\boldsymbol{\xi} = \mathbf{0}$ is UGES.

The guidance system (10) is considered next. Since $\boldsymbol{\nu}_c = \boldsymbol{R}^T(\psi)\boldsymbol{V}_c$ and $\tilde{\psi} \triangleq \psi - \psi_d$, the integrator (10b) can be written as:

$$\dot{v}_{\text{int}} = -V_x \sin(\psi_d + \tilde{\psi}) + V_y \cos(\psi_d + \tilde{\psi}), \tag{15}$$

where $\psi_d = -\sigma v_{\text{int}}$. The interconnected dynamics of v_{int} are given combining (15) with (14):

$$\begin{aligned} \dot{v}_{\text{int}} &= V_x \sin(\sigma v_{\text{int}}) + V_y \cos(\sigma v_{\text{int}}) \\ &\quad + \boldsymbol{H}_v(v_{\text{int}}, \boldsymbol{\xi})\boldsymbol{\xi}, \end{aligned} \tag{16a}$$

$$\dot{\boldsymbol{\xi}} = \boldsymbol{\Sigma}\boldsymbol{\xi}, \tag{16b}$$

where $\boldsymbol{H}_v(v_{\text{int}}, \boldsymbol{\xi}) \triangleq [h_{v_{\text{int}}}(v_{\text{int}}, \tilde{\psi}),\ 0]$ and the function $h_{v_{\text{int}}}(v_{\text{int}}, \tilde{\psi})$ is given in Appendix A. The system (16) is a cascaded system where the linear UGES system (16b) perturbs the dynamics (16a) through the interconnection term $\boldsymbol{H}_v$. Analyzing (16) at equilibrium shows that $\boldsymbol{\xi}^{\text{eq}} = \mathbf{0}$ and:

$$V_x \sin(\sigma v_{\text{int}}^{\text{eq}}) + V_y \cos(\sigma v_{\text{int}}^{\text{eq}}) = 0, \tag{17}$$

therefore:

$$v_{\text{int},k}^{\text{eq}} = -(1/\sigma)\left[\text{atan2}\left(V_y, V_x\right) + k\pi\right], \quad k \in \mathbb{Z}. \tag{18}$$

The system (16) has multiple equilibrium points that identify two physical directions: the counter-current direction and the co-current direction. This is clearly seen if the course held by the ship at equilibrium is calculated:

$$\psi_k^{\text{eq}} = \text{atan2}\left(V_y, V_x\right) + k\pi, \quad k \in \mathbb{Z}, \tag{19}$$

where the equilibrium points with $k = 1 + 2n, n \in \mathbb{Z}$ correspond to the counter-current direction, while the equilibrium points identified by $k = 2n, n \in \mathbb{Z}$ correspond to the co-current direction. In particular, the equilibrium point with $k = 1$ that corresponds to the counter-current course, $v_{\text{int},1}^{\text{eq}}$, is considered.

Remark 7. The equilibrium point having $k = 1$ is equivalent to all the counter-current equilibrium points identified by $k = 1 + 2n, n \in \mathbb{Z}$, hence their analysis is identical.

The variable $e \triangleq v_{\text{int}} - v_{\text{int},1}^{\text{eq}}$ is introduced to move the equilibrium point to the origin. This is in fact a rotation of the inertial frame i for an angle ψ_1^{eq}. The cascaded system (16) can be then rewritten in the following form:

$$\dot{e} = -V_c \sin(\sigma e) + \boldsymbol{H}_e(e, \boldsymbol{\xi})\boldsymbol{\xi}, \tag{20a}$$

$$\dot{\boldsymbol{\xi}} = \boldsymbol{\Sigma}\boldsymbol{\xi}, \tag{20b}$$

where $V_c > 0$ is the magnitude of the ocean current, $V_c \triangleq \sqrt{V_x^2 + V_y^2}$, and $\boldsymbol{H}_e \triangleq [h_e(e, \tilde{\psi}),\ 0]$. The function $h_e(e, \tilde{\psi})$ is given in Appendix A.

From this point on the proof differs consistently from Caharija et al. (2014): the positive definite quadratic Lyapunov function candidate (LFC) from (Caharija et al., 2014, Lemma 3) is applied to (20) in a direct attempt to prove stability instead of boundedness only as done in the aforementioned Lemma. The LFC is:

$$W_1 \triangleq \boldsymbol{\chi}^T \boldsymbol{P} \boldsymbol{\chi}, \tag{21}$$

where $\boldsymbol{\chi} \triangleq [e, \tilde{\psi}, \tilde{r}]^T$ and the matrix $\boldsymbol{P}$ is defined as:

$$\boldsymbol{P} \triangleq \begin{bmatrix} \frac{1}{2} & 0 & 0 \\ 0 & \frac{\rho}{2}\left[\frac{k_\psi}{k_r}\left(1+\frac{1}{k_\psi}\right)+\frac{k_r}{k_\psi}\right] & \frac{\rho}{2k_\psi} \\ 0 & \frac{\rho}{2k_\psi} & \frac{\rho}{2k_r}\left(1+\frac{1}{k_\psi}\right) \end{bmatrix}, \tag{22}$$

where $\rho > 0$ is a constant parameter. Notice that the matrix $\boldsymbol{P}$ is symmetric and positive definite. Hence, its eigenvalues $\lambda_1, \lambda_2, \lambda_3$ are real and positive. In particular $\lambda_1 = 1/2$ and the other two are linearly dependent on ρ: $\lambda_2(\rho) = c_2(k_\psi, k_r)\rho$ and $\lambda_3(\rho) = c_3(k_\psi, k_r)\rho$, where $c_2(k_\psi, k_r) > 0$ and $c_3(k_\psi, k_r) > 0$ are given in Appendix A. The time derivative of the LFC (21) is:

$$\dot{W}_1 = -\rho\tilde{\psi}^2 - \rho\tilde{r}^2 - V_c e \sin(\sigma e) + e\tilde{\psi}h(e, \tilde{\psi}). \tag{23}$$

Notice that the function $h(e, \tilde{\psi})$ is globally bounded, since $|h(e, \tilde{\psi})| \leq 2V_{\max}$. Therefore, in any ball $\mathcal{B}_{1/\sigma} \triangleq \{|e| \leq 1/\sigma\}$, the time-derivative of W_1 satisfies the following inequality:

$$\dot{W}_1 \leq -\rho\tilde{\psi}^2 - \rho\tilde{r}^2 - V_{\max}\sigma\frac{e^2}{2} + 2V_{\max}|e||\tilde{\psi}|. \tag{24}$$

The bound (24) can be rewritten as:

$$\dot{W}_1 \leq -W_B(|\tilde{r}|, |e|, |\tilde{\psi}|), \tag{25}$$

where:

$$W_B(|\tilde{r}|, |e|, |\tilde{\psi}|) \triangleq \begin{bmatrix} |\tilde{r}| & |e| & |\tilde{\psi}| \end{bmatrix} \begin{bmatrix} \rho & 0 & 0 \\ 0 & \frac{V_{\max}\sigma}{2} & -V_{\max} \\ 0 & -V_{\max} & \rho \end{bmatrix} \begin{bmatrix} |\tilde{r}| \\ |e| \\ |\tilde{\psi}| \end{bmatrix} \tag{26}$$

It is straightforward to show that W_B is positive definite as long as $\rho > \frac{2V_{\max}}{\sigma}$. Without any loss of generality one can choose for instance $\rho = \frac{3V_{\max}}{\sigma}$, hence making two of the eigenvalues of W_1 linearly dependent on $1/\sigma$ and all the eigenvalues of W_B dependent on $1/\sigma$. Given that the tuning parameter $\sigma > 0$ can be chosen arbitrarily small, this shows exponential stability on a domain of

attraction that can be made arbitrarily large by picking σ small enough. Therefore, according to (Grøtli et al., 2008, Theorem 2), it is possible to conclude uniform semiglobal exponential stability on the parameter set $\Theta = \{\sigma > 0\}$ for the system (20).

Remark 8. The precise definition of the USES stability property is given in Grøtli et al. (2008).

Remark 9. Even though the equilibria of (20) are multiple, they all can be separated by an arbitrarily large distance by picking $\sigma > 0$ small enough. This explains intuitively why the stability properties of (20) hold semiglobally.

Hence, following Remark 7, all the counter-current equilibrium points ($k = 1 + 2n, n \in \mathbb{Z}$) have USES and stability properties. Moreover, linearisation shows instability of the equilibrium points identifying the co-current direction ($k = 2n, n \in \mathbb{Z}$). Finally, ISS for the sway dynamics (5e) can be shown as done in Caharija et al. (2014) by exploiting Assumption 4 in combination with the fact that u_r is bounded, as guaranteed by the controller (11). To conclude, the guidance law (10) in a cascaded configuration with the controllers (11-12) guarantee USES on the parameter set $\Theta = \{\sigma > 0\}$ of the counter-current equilibrium points ($k = 1 + 2n, n \to \mathbb{Z}$) of the closed loop system (20). Hence, for any ball of initial conditions $\boldsymbol{\chi}_o$ there exists a small enough $\sigma > 0$ such that the objectives (7-9) are achieved exponentially.

Similarly, the same proof can be repeated for the co-current guidance ($\sigma < 0$).

7. SIMULATIONS

In this section results from numerical simulations are presented where the counter-current/co-current guidance law (10) is applied to the HUGIN AUV. The objective is to make the vehicle move against the sea current or, complementary, follow the sea current and hold a desired surge relative speed $U_{rd} = 1$ m/s. Notice that the guidance law sets the heading of the vessel only, while its position is unconstrained. The current components are $V_x = -0.41$ m/s and $V_y = 0.29$ m/s, giving an intensity of $|\boldsymbol{V}_c| = 0.5$ m/s and a direction of 144.2 deg. Thus, Assumptions 1 and 5 are fulfilled with $V_{\max} = 0.5$ m/s. Furthermore, it can be verified that Assumption 4 is satisfied with $Y^{\min} = 0.60$ s^{-1} and $X^{\max} = 1.08$ m/s.

The chosen values for the gain σ in the counter-current case and in the co-current case are 0.1 m^{-1} and -0.1 m^{-1}, respectively. Choosing too high values for σ may induce chattering due to saturation in the magnitude and the turning rate of the rudder actuators. Linearising the system (20) at the origin shows that the convergence rate of the guidance law is in first approximation dependent on the constant σV_c. Given that $V_c = 0.5$ m/s and $|\sigma| = 0.1$ m^{-1}, this gives a time constant of 20 s. In particular, the restoring term $V_c \sin(\sigma e)$ is strongest at the origin, thus the guidance dynamics are faster close to the stable equilibrium point. The internal controllers (11-12) are implemented with the following gains: $k_{u_r} = 0.7$, $k_\psi = 1$ and $k_r = 2$. Hence, the $\tilde{u}_r$ first order closed loop system (13) has a time constant of 1.4 s while the $\tilde{\psi}$ second order closed loop system (14) is critically damped with $\omega_n = 1$ rad/s. The yaw closed loop system is made critically damped to have the fastest possible response without overshoots.

The AUV is initially located at the origin of the inertial frame and holds zero relative velocity. Its surge axis is parallel to the x axis of the inertial frame. Figures A.1 and A.4 show how counter-current and co-current guidance are successfully achieved. Notice that the current is acting in the 144.2 deg direction and that the guidance law correctly identifies the counter-current course as well as the co-current course (Figures A.2 and A.5). Figures A.3 and A.6 show the relative sway velocity and the sway current component over time in the two cases. As expected, the sway current component converges to zero since it is the error signal of the guidance law. The practical implementability of the counter-current/co-current guidance can be assessed by analysing the rudder angle of the vessel from Figures A.2 and A.5. This illustrates that the proposed guidance is implementable as long as reliable measurements of the v_c current component are available. Notice that in the simulations saturation is taken into account for both the rudder and the propeller.

8. CONCLUSIONS

In this paper stronger stability properties have been shown for the counter-current and co-current guidance of underactuated marine vehicles that was first presented in Caharija et al. (2014). In particular, the USES stability property was shown for the complete multiple-equilibria closed-loop system, that was previously shown to be only uniformly aemiglobally asymptotically stable (USAS) and locally uniformly locally exponentially stable (ULES). Compared to Caharija et al. (2014), the proof presented in this paper did not invoke the theory developed for cascaded systems in Chaillet and Loría (2008). Instead, a direct approach was followed where a Lyapunov function for the full system was identified. This proves that applying the direct Lyapunov method to analyse the stability of complex non-linear systems can lead to significant results, despite the difficulty of identifying the right Lyapunov function candidate. Finally, numerical simulations using a high-fidelity model of the HUGIN AUV were shown to support the theoretical results.

REFERENCES

Aguiar, A. and Pascoal, A.M. (1997). Modeling and control of an autonomous underwater shuttle for the transport of benthic laboratories. In *Proc. of MTS/IEEE Conference OCEANS '97*, 888–895.

Antonelli, G. (2007). On the use of adaptive/integral actions for six-degrees-of-freedom control of autonomous underwater vehicles. *IEEE Journal of Oceanic Engineering*, 32(2), 300–312.

Batista, P., Silvestre, C., and Oliveira, P. (2012). GES integrated LBL/USBL navigation system for underwater vehicles. In *Proc. of the IEEE 51st Conference on Decision and Control*, 6609–6614.

Breivik, M. and Fossen, T.I. (2009). *Guidance Laws for Autonomous Underwater Vehicles*, chapter 4, 51–76. A. V. Inzartsev, IN-TECH Education and Publishing.

Børhaug, E., Pavlov, A., and Pettersen, K.Y. (2008). Integral LOS control for path following of underactuated

marine surface vessels in the presence of constant ocean currents. In *Proc. of the 47th IEEE Conference on Decision and Control*, 4984–4991.

Caharija, W., Grøtli, E.I., and Pettersen, K.Y. (2014). Improved counter-current and co-current guidance of underactuated marine vehicles with semiglobal stability properties. In *Proc. of the 19th IFAC World Congress*, 12166–12173.

Caharija, W., Pettersen, K.Y., Bibuli, M., Calado, P., Zereik, E., Braga, J., Gravdahl, J.T., Sørensen, A.J., Milovanović, M., and Bruzzone, G. (2016). Integral line-of-sight guidance and control of underactuated marine vehicles: Theory, simulations, and experiments. *IEEE Transactions on Control Systems Technology*, 24(5), 1623–1642.

Caharija, W., Pettersen, K.Y., and Gravdahl, J.T. (2013). Counter-current and co-current guidance of underactuated unmanned marine vehicles. In *Proc. of the 8th IFAC Symposium on Intelligent Autonomous Vehicles*, 184–191.

Chaillet, A. and Loría, A. (2008). Uniform semiglobal practical asymptotic stability for non-autonomous cascaded systems and applications. *Automatica*, 44(2), 337–347.

Do, K.D., Pan, J., and Jiang, Z.P. (2004). Robust and adaptive path following for underactuated autonomous underwater vehicles. *Ocean Engineering*, 31, 1967–1997.

Encarnação, P., Pascoal, A.M., and Arcak, M. (2000). Path following for marine vehicles in the presence of unknown currents. In *Proc. of the 6th IFAC International Symposium on Robot Control*, 469–474.

Fossen, T.I. (2011). *Handbook of Marine Craft Hydrodynamics and Motion Control*. John Wiley & Sons, Inc., Hoboken, NJ.

Fossen, T.I. and Lekkas, A.M. (2017). Direct and indirect adaptive integral line-of-sight path-following controllers for marine craft exposed to ocean currents. *International Journal of Adaptive Control and Signal Processing*, 31, 445–463.

Fossen, T.I. and Strand, J.P. (2001). Nonlinear passive weather optimal positioning control (WOPC) system for ships and rigs: experimental results. *Automatica*, 37(5), 701–715.

Fredriksen, E. and Pettersen, K.Y. (2004). Global κ-exponential way-point manoeuvering of ships. In *Proc. of the 43rd IEEE Conference on Decision and Control*, 5360–5367.

Grøtli, E.I., Chaillet, A., and Gravdahl, J.T. (2008). Output control of spacecraft in leader follower formation. In *Proc. of the 47th IEEE Conference on Decision and Control*, 1030–1035.

Indiveri, G., Creti, S., and Zizzari, A.A. (2012). A proof of concept for the guidance of 3D underactuated vehicles subject to constant unknow disturbances. In *Proc. of the 9th IFAC Conference on Manoeuvring and Control of Marine Crafts*.

Jouffroy, J., Zhou, Q., and Zielinski, O. (2011). Towards selective tidal-stream transport for lagrangian profilers. In *Proc. of MTS/IEEE Conference OCEANS '11*, 1–6.

Kim, Y.S., Kim, J., and Sung, H.G. (2016). Weather-optimal control of a dynamic positioning vessel using backstepping: simulation and model experiment. In *10th IFAC Conference on Control Applications in Marine Systems*, 232–238.

Kim, Y.S., Lee, H., and Kim, J. (2017). Coordinated weathervaning control of two surface vessels in a tandem configuration. *Ocean Engineering*, 130, 142–155.

Kjerstad, .K. and Breivik, M. (2010). Weather optimal positioning control for marine surface vessels. In *Proc. of the 8th IFAC Conference on Control Applications in Marine Systems*.

Paliotta, C., Lefeber, E., and Pettersen, K.Y. (2016). Trajectory tracking of under-actuated marine vehicles. In *Proc. of 2016 IEEE 55th Conference on Decision and Control*, 5660–5667.

Smith, R.N., Schwager, M., Smith, S.L., Jones, B.H., Rus, D., and Sukhatme, G.S. (2011). Persistent ocean monitoring with underwater gliders: Adapting sampling resolution. *Journal of Field Robotics*, 28(5), 714–741.

Zheng, J., Wan, L., Li, Y., Dong, Z., and Zhang, Y. (2017). Adaptive line-of-sight path following control for underactuated autonomous underwater vehicles in the presence of ocean currents. *International Journal of Advanced Robotic Systems*.

Appendix A

$$\boldsymbol{R}(\psi) \triangleq \begin{bmatrix} \cos(\psi) & -\sin(\psi) & 0 \\ \sin(\psi) & \cos(\psi) & 0 \\ 0 & 0 & 1 \end{bmatrix}, \tag{A.1}$$

$$\boldsymbol{M} \triangleq \begin{bmatrix} m_{11} & 0 & 0 \\ 0 & m_{22} & m_{23} \\ 0 & m_{23} & m_{33} \end{bmatrix}, \quad \boldsymbol{B} \triangleq \begin{bmatrix} b_{11} & 0 \\ 0 & b_{22} \\ 0 & b_{32} \end{bmatrix}, \tag{A.2}$$

$$\boldsymbol{C}(\boldsymbol{\nu}_r) \triangleq \begin{bmatrix} 0 & 0 & -m_{22}v_r - m_{23}r \\ 0 & 0 & m_{11}u_r \\ m_{22}v_r + m_{23}r & -m_{11}u_r & 0 \end{bmatrix}, \tag{A.3}$$

$$F_{u_r}(v_r, r) \triangleq \frac{1}{m_{11}}(m_{22}v_r + m_{23}r)r, \tag{A.4}$$

$$X(u_r) \triangleq \frac{m_{23}^2 - m_{11}m_{33}}{m_{22}m_{33} - m_{23}^2}u_r + \frac{d_{33}m_{23} - d_{23}m_{33}}{m_{22}m_{33} - m_{23}^2}, \tag{A.5}$$

$$Y(u_r) \triangleq \frac{(m_{22} - m_{11})m_{23}}{m_{22}m_{33} - m_{23}^2}u_r - \frac{d_{22}m_{33} - d_{32}m_{23}}{m_{22}m_{33} - m_{23}^2}, \tag{A.6}$$

$$\begin{aligned} F_r(u_r, v_r, r) \triangleq{}& \frac{m_{23}d_{22} - m_{22}(d_{32} + (m_{22} - m_{11})u_r)}{m_{22}m_{33} - m_{23}^2}v_r \\ &+ \frac{m_{23}(d_{23} + m_{11}u_r) - m_{22}(d_{33} + m_{23}u_r)}{m_{22}m_{33} - m_{23}^2}r. \end{aligned} \tag{A.7}$$

The functions $h_{v_{\text{int}}}(v_{\text{int}}, \tilde{\psi})$, $h_e(e, \tilde{\psi})$, $c_2(k_\psi, k_r)$ and $c_3(k_\psi, k_r)$ are:

$$\begin{aligned} h_{v_{\text{int}}}(v_{\text{int}}, \tilde{\psi}) \triangleq{}& -\frac{1 - \cos(\tilde{\psi})}{\tilde{\psi}}\left(V_x \sin(\sigma v_{\text{int}}) + V_y \cos(\sigma v_{\text{int}})\right) \\ &- \frac{\sin(\tilde{\psi})}{\tilde{\psi}}\left(V_x \cos(\sigma v_{\text{int}}) - V_y \sin(\sigma v_{\text{int}})\right), \end{aligned} \tag{A.8}$$

$$h_e(e, \tilde{\psi}) \triangleq V_c \frac{1 - \cos(\tilde{\psi})}{\tilde{\psi}} \sin(\sigma e) + V_c \frac{\sin(\tilde{\psi})}{\tilde{\psi}} \cos(\sigma e), \tag{A.9}$$

$$c_{2,3}(k_\psi, k_r) \triangleq \frac{1}{4}\left(\frac{k_\psi + 2}{k_r} + \frac{k_r}{k_\psi} + \frac{1}{k_\psi k_r}\right)\left\{1 \right. \tag{A.10}$$

$$\left. \pm \sqrt{1 - \frac{4k_\psi}{(k_\psi + 1)^2 + k_r^2}}\right\}, \tag{A.11}$$

where the limits of $h_{v_{\text{int}}}$ and h_e for $\tilde{\psi} \to 0$ exist and are finite. The constant $V_c > 0$ is the magnitude of the current: $V_c \triangleq \sqrt{V_x^2 + V_y^2}$. Notice that the following identities are used when moving the equilibrium point $v_{\text{int},1}^{\text{eq}}$ to the origin in Section 6 (recall that $e = v_{\text{int}} - v_{\text{int},1}^{\text{eq}}$):

$$V_x \sin(\sigma v_{\text{int}}) + V_y \cos(\sigma v_{\text{int}}) = -V_c \sin(\sigma e), \tag{A.12}$$

$$V_x \cos(\sigma v_{\text{int}}) - V_y \sin(\sigma v_{\text{int}}) = -V_c \cos(\sigma e), \tag{A.13}$$

$$\sin(\text{atan2}\,(V_y, V_x)) = V_y / V_c, \tag{A.14}$$

$$\cos(\text{atan2}\,(V_y, V_x)) = V_x / V_c. \tag{A.15}$$

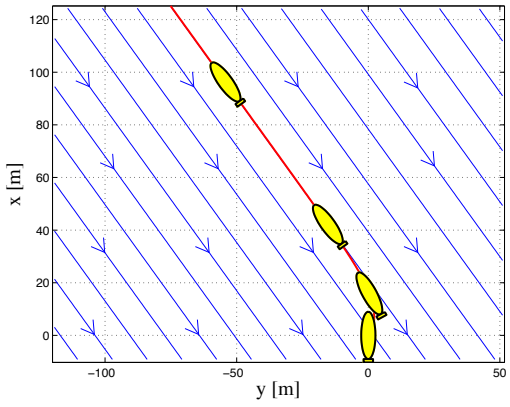

Fig. A.1. Counter-current guidance of the underactuated HUGIN AUV ($\sigma = 0.1$ [m^{-1}]).

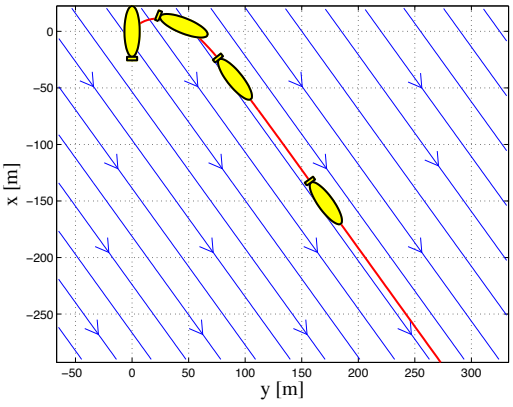

Fig. A.4. Co-current guidance of the underactuated HUGIN AUV ($\sigma = -0.1$ m^{-1}).

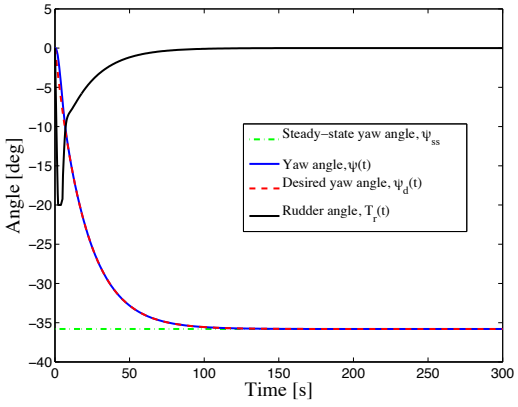

Fig. A.2. Yaw angle $\psi(t)$ of the vehicle in counter-current guidance mode ($\sigma = 0.1$ m^{-1}). Notice that the steady state yaw angle is $\psi_{ss} = -35.8$ deg while the current is acting in exactly the opposite direction of 144.2 deg.

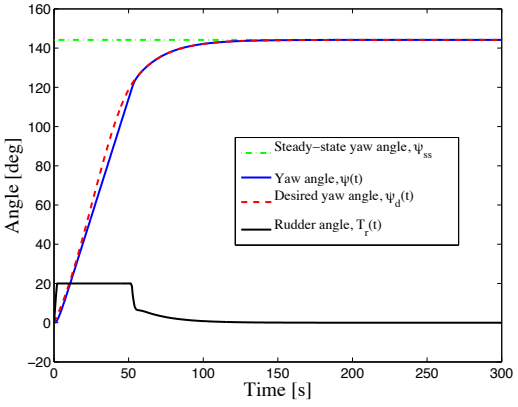

Fig. A.5. Yaw angle $\psi(t)$ of the vehicle in co-current guidance mode ($\sigma = -0.1$ m^{-1}). Notice that the steady state yaw angle is $\psi_{ss} = 144.2$ deg which is exactly the current direction.

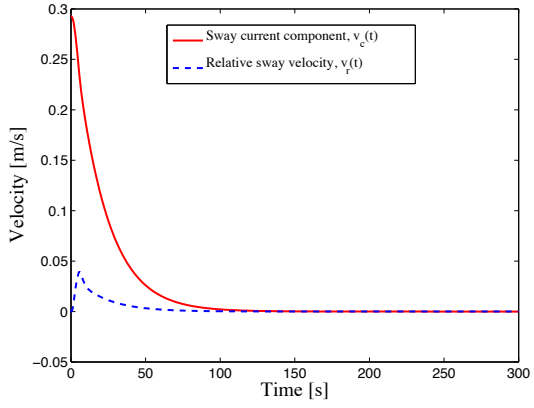

Fig. A.3. The relative and absolute sway velocities of the AUV and the sway current component in counter-current guidance mode converge to zero as expected ($\sigma = 0.1$ m^{-1}).

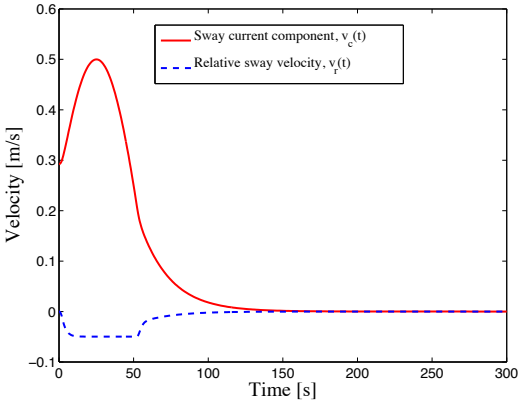

Fig. A.6. The relative and absolute sway velocities of the AUV and the sway current component in co-current guidance mode converge to zero as expected ($\sigma = -0.1$ m^{-1}).